Chinese Chemical Letters 37 (2026) 112139

Contents lists available at ScienceDirect

Chinese Chemical Letters

journal homepage: www.elsevier.com/locate/cclet

Surface modification of iron oxide nanoparticles for enhanced therapeutic efficacy in inflammatory bowel disease

Mengjie Wang[a,b,1], Shilin Li[a,c,1], Manman Ning[a,1], Yueguang Xue[a,d], Ke Xu[a,c], Xinran Wang[e], Shasha Jiang[f,*], Yongfu Ma[g,*], Ying Liu[a,*]

[a] CAS Key Laboratory for Biomedical Effects of Nanomaterials and Nanosafety & CAS Center for Excellence in Nanoscience, National Center for Nanoscience and Technology of China, Beijing 100190, China
[b] Hangzhou Institute of Medicine, Chinese Academy of Sciences, Hangzhou 310006, China
[c] University of Chinese Academy of Sciences, Beijing 100049, China
[d] School of Biomedical Sciences and Engineering, South China University of Technology, Guangzhou 511442, China
[e] The Hong Kong University of Science and Technology, Hong Kong 999077, China
[f] The 990th Hospital of the Jointservice Support Force of the PLA, Zhumadian 463000, China
[g] Department of Thoracic Surgery, the First Medical Center of Chinese PLA General Hospital, Beijing 100853, China

ARTICLE INFO

Article history:
Received 28 June 2025
Revised 18 November 2025
Accepted 20 November 2025
Available online 20 November 2025

Keywords:
Inflammatory bowel disease
Iron oxide nanoparticle
Protein corona
Surface modification
Multicellular model

ABSTRACT

Inflammatory bowel disease (IBD) is a chronic condition that severely affects the gastrointestinal tract. Current treatments often have limited efficacy and significant side effects. Iron oxide nanoparticles (Fe_2O_3 NPs) have emerged as promising candidates for IBD therapy due to their biocompatibility and stability. This study investigates how different surface modifications influence the therapeutic efficacy of Fe_2O_3 NPs in IBD management. We developed four different types of modified Fe_2O_3 NPs, including unmodified γ-Fe_2O_3 NPs, amine-functionalized Fe_2O_3 NPs (APTS-Fe_2O_3 NPs), poly-L-lysine-coated Fe_2O_3 NPs (PLL-Fe_2O_3 NPs), and dimercaptosuccinic acid-coated Fe_2O_3 NPs (DMSA-Fe_2O_3 NPs). Our results demonstrate that all types of Fe_2O_3 NPs can adsorb proteins to form the protein corona. However, the composition of the protein corona varies, leading to different therapeutic effects of the NPs on IBD. Among them, APTS-Fe_2O_3 NPs showed reduced therapeutic efficacy compared to the other surface-modified NPs. This was attributed to their adsorption of higher levels of protective and translocation-related proteins, as well as enhanced permeability across intestinal epithelial cells. These findings underscore the importance of carefully tailoring nanoparticle surface properties. Overall, this study highlights the significance of understanding nanoparticle-protein interactions in designing more effective nanoparticle-based therapies for IBD.

© 2026 Published by Elsevier B.V. on behalf of Chinese Chemical Society and Institute of Materia Medica, Chinese Academy of Medical Sciences.

Inflammatory bowel disease (IBD), encompassing Crohn's disease and ulcerative colitis (UC), is a chronic inflammatory condition of the gastrointestinal tract with an unclear etiology and complex pathogenesis [1,2]. It is widely thought to arise from an interplay of genetic predisposition, immune dysregulation, environmental factors, and gut microbiota dysbiosis [3], contributing to substantial patient morbidity [4–6]. Current IBD therapies include immunomodulators (*e.g.*, azathioprine (Imuran) and methotrexate), biologics (*e.g.*, tumor necrosis factor-alpha (TNF-α) antibodies), fecal microbiota transplantation (FMT), and corticosteroids [7]. While these treatments effectively control inflammation and alleviate symptoms, they are associated with notable limitations, and many patients experience relapses and significant side effects from conventional therapies [8,9]. Consequently, there is a critical need for new therapeutic strategies that can more effectively manage IBD with fewer adverse effects [7,10].

Protein adsorption therapy represents a promising approach for IBD by selectively removing inflammatory cytokines or harmful proteins from the intestinal lumen. This strategy offers rapid relief from inflammation while reducing systemic drug-related side effects [11]. Despite its localized effects, traditional adsorption materials face several limitations, such as poor biocompatibility, potential disruption of normal intestinal proteins, and generally insufficient adsorption capacity to meet the long-term therapeutic demands of IBD patients [12]. Recent advances in nanotechnol-

* Corresponding authors.
E-mail addresses: jiangshasha1114@163.com (S. Jiang), yongfuabc@sina.com (Y. Ma), liuy@nanoctr.cn (Y. Liu).
[1] These authors contributed equally to this work.

https://doi.org/10.1016/j.cclet.2025.112139
1001-8417/© 2026 Published by Elsevier B.V. on behalf of Chinese Chemical Society and Institute of Materia Medica, Chinese Academy of Medical Sciences.

ogy have opened new possibilities for the treatment of inflammatory diseases, including IBD [13,14]. Among various nanomaterials, iron oxide NPs (Fe_2O_3 NPs) have attracted considerable interest due to their biocompatibility, chemical stability, magnetic properties, ease of surface modification, and potential to modulate immune responses [15–17]. Originally explored in oncology [18–20], Fe_2O_3 NPs have shown therapeutic potential in IBD by mitigating oxidative stress through scavenging reactive oxygen species (ROS), thereby protecting intestinal epithelial cells [21,22]. Their high surface area and modifiable surfaces also enable efficient adsorption of key inflammatory mediators such as TNF-α and interleukin-6 (IL-6) [23]. Furthermore, the enhanced stability of Fe_2O_3 NPs allows for the slow release of iron ions in the gut, thereby improving absorption efficiency and positioning them as a novel iron supplementation strategy for IBD patients [24]. The multifunctional surface of iron oxide NPs enables the binding of biomolecules and drug, allowing for targeted diagnosis and treatment [25]. The combined properties make Fe_2O_3 NPs a promising therapeutic strategy for IBD management.

Surface modification plays a critical role in regulating the biological interactions, stability, and therapeutic performance of NPs [26]. By modifying the surface of Fe_2O_3 NPs with different functional groups, it is possible to enhance their specific targeting, reduce immunogenicity, and improve their therapeutic outcomes [27,28]. In this study, we prepared and compared four types of Fe_2O_3 NPs with distinct surface modifications: Unmodified γ-Fe_2O_3 NPs, amine-functionalized Fe_2O_3 NPs (APTS-Fe_2O_3 NPs), poly-L-lysine-coated Fe_2O_3 NPs (PLL-Fe_2O_3 NPs), and dimercaptosuccinic acid-coated Fe_2O_3 NPs (DMSA-Fe_2O_3 NPs). This selection encompasses both inorganic-modified groups with positive and negative surface charges, along with PLL as a representative organic polymer coating, thereby providing a comprehensive and representative assessment of how surface chemistry influences nanoparticle behavior. We systematically investigated the effects of these surface modifications on the therapeutic efficacy of Fe_2O_3 NPs in IBD, focusing particularly on the molecular mechanisms by which they alter intestinal epithelial cell permeability and modulate the ensuing inflammatory response. By elucidating these mechanisms, our study aims to guide the rational design of Fe_2O_3 NPs for improved therapeutic outcomes in IBD and to provide insights for developing more effective nanoparticle-based therapies for IBD and other inflammatory diseases.

Four types of surface-modified iron oxide NPs were synthesized using established methods. Dynamic light scattering (DLS) revealed that the hydrodynamic sizes and polydispersity index (PDI) of γ-Fe_2O_3, DMSA-Fe_2O_3, APTS-Fe_2O_3, and PLL-Fe_2O_3 NPs to be approximately 82 nm/0.171, 76.67 nm/0.2, 104.7 nm/0.236, and 84.62 nm/0.294, respectively (Figs. 1A–D). The corresponding zeta potentials were measured as +38.6, −31.7, +29.3, and +51.9 mV, respectively (Fig. S1A in Supporting information), consistent with their surface modifications. Transmission electron microscope (TEM) images confirmed that individual Fe_2O_3 NPs were spherical, with primary particle sizes ranging from 10 nm to 20 nm. Although unfunctionalized Fe_2O_3 NPs typically exhibit a negative surface charge, the unmodified γ-Fe_2O_3 NPs here showed a positive zeta potential (+38.6 mV), attributable to protonation during nitric acid treatment in the synthesis process. Despite the initial positive charge, subsequent functionalization with the positively charged ligands APTS and PLL was successfully carried out under specifically controlled acidic conditions (pH 3–4 for APTS and pH 2.0 for PLL). Successful surface modification was further verified by Fourier-transform infrared (FTIR) spectroscopy, which confirmed the presence of APTS, carboxylic groups (from DMSA), and PLL on the respective γ-Fe_2O_3 NP surfaces (Figs. 1A–D).

Thermogravimetric (TG) analysis indicated that all four types of surface-modified Fe_2O_3 NPs exhibited thermal stability below

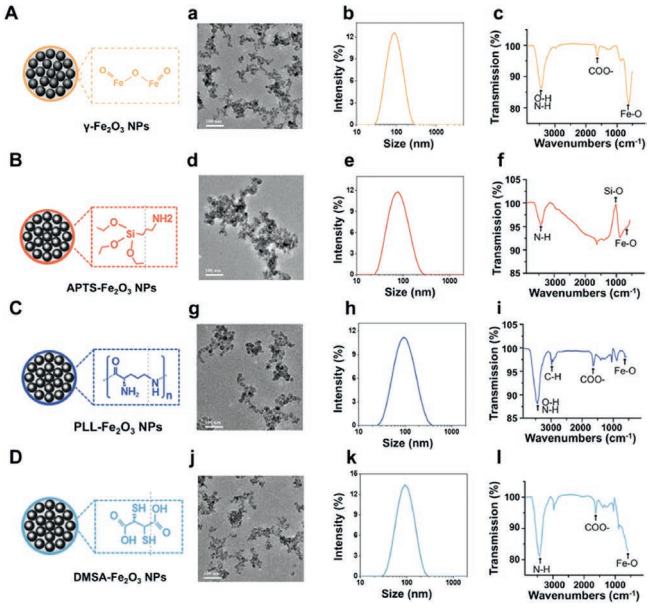


Fig. 1. Synthesis and characterization of iron oxide NPs (Fe_2O_3 NPs) with different surface modifications. (A) γ-Fe_2O_3, (B) APTS-Fe_2O_3, (C) PLL-Fe_2O_3, (D) DMSA-Fe_2O_3 by TEM (a, d, g, j), DLS (b, e, h, k), and FTIR (c, f, i, l), respectively. Scale bar: 100 nm.

250 °C, with a weight loss of <5%. As the temperature increased to 900 °C, γ-Fe_2O_3, APTS-Fe_2O_3, and PLL-Fe_2O_3 NPs displayed a stable weight loss of ~7%, indicating strong thermal stability. In contrast, DMSA-Fe_2O_3 NPs underwent more substantial weight loss near 300 and 600 °C, reaching 13% at 900 °C, which suggests partial decomposition (Fig. S1B in Supporting information). Despite being less stable than the other three variants, DMSA-Fe_2O_3 NPs still maintained overall good stability. X-ray photoelectron spectroscopy (XPS) analysis detected characteristic peaks corresponding to Na, O, Fe, and Cl in γ-Fe_2O_3 NPs. The Fe $2p_{1/2}$ and Fe $2p_{3/2}$ transitions confirmed that iron primarily existed in Fe^{3+} oxidation state (Fig. S1C in Supporting information). Furthermore, cell counting kit-8 (CCK-8) assays conducted in Caco-2 cells revealed no significant cytotoxicity of Fe_2O_3 NPs at concentrations up to 200 μg/mL after 72 h of exposure, confirming their good biocompatibility (Fig. S1D in Supporting information).

To evaluate the therapeutic potential of Fe_2O_3 NPs in IBD, animal experiments were performed under the approval of the Institutional Animal Care and Use Committee of the National Center for Nanoscience and Technology (approval ID: NCNST21–202412–0126). Acute UC was induced in mice *via* oral administration of 2% dextran sulfate sodium (DSS). Within three days, the mice developed weight loss and mild fecal occult blood, with symptoms progressively worsening (Fig. 2A and Fig. S2A in Supporting information). By day 7, body weight had decreased by approximately 20%, accompanied by reduced activity and severe occult bleeding, confirming the successful establishment of the colitis model. After DSS withdrawal, the mice showed partial weight recovery, which was followed by a subsequent decline, indicating limited self-repair. Treatment with γ-Fe_2O_3, PLL-Fe_2O_3, or DMSA-Fe_2O_3 NPs restored body weight to nearly pre-model levels. Although APTS-Fe_2O_3 NPs did not completely reverse weight loss, they prevented further deterioration compared with the control group, suggesting a moderate anti-inflammatory effect (Fig. 2B).

Survival analysis revealed no mortality in the normal, PLL-Fe_2O_3 NP, and DMSA-Fe_2O_3 NP groups. In contrast, mortality rates were 8.33% in the γ-Fe_2O_3 NP group and 25% in both the water and APTS-Fe_2O_3 NP groups (Fig. 2C). Following treatment, the disease activity index (DAI) scores consistently decreased in the γ-Fe_2O_3,

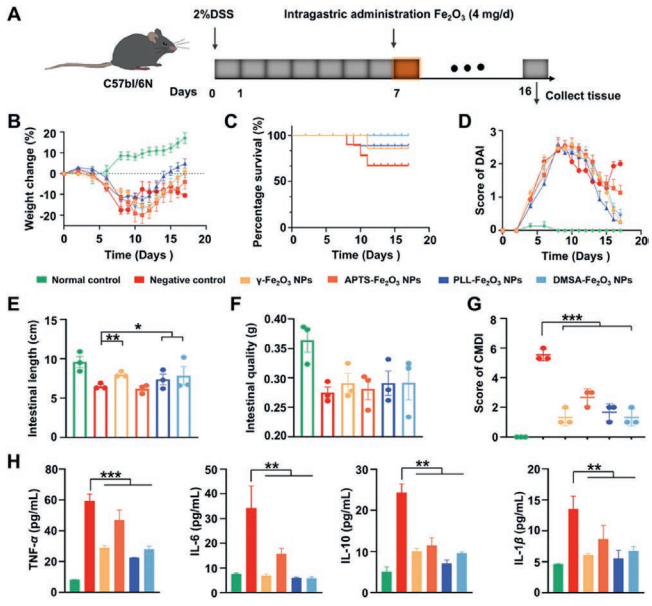


Fig. 2. Evaluation of the therapeutic effects of Fe_2O_3 NPs on DSS-induced acute UC in mice. (A) The scheme figure for animal experiments. (B) Body weight change and (C) survival curves of the different experimental groups. (D) The DAI score assesses weight loss, stool consistency, and bleeding in the different experimental groups. (E) DSS-induced colon shortening was markedly ameliorated by Fe_2O_3 NPs. (F) Colon weight measurement of the different experimental groups. (G) DSS-induced colonic mucosal damage was markedly ameliorated by Fe_2O_3 NPs. (H) The serum inflammatory factor levels in different groups. $^{*}P < 0.05$, $^{**}P < 0.01$, $^{***}P < 0.001$. Data are presented as mean ± standard deviation (SD) ($n = 3$).

PLL-Fe_2O_3, and DMSA-Fe_2O_3 NP groups. Mice in the water and APTS-Fe_2O_3 NP groups exhibited an initial decline in DAI from days 1 to 7, which was followed by fluctuations and a rebound on days 8–9. Notably, the DAI increase in the APTS-Fe_2O_3 NP group was slightly lower than that in the water group (Fig. 2D), suggesting a modest, though limited, anti-inflammatory effect of APTS-modified NPs compared to the other Fe_2O_3 NP formulations. Assessment of intestinal length (cecum + colon + rectum) showed that oral administration of γ-Fe_2O_3 NPs, PLL-Fe_2O_3 NPs, and DMSA-Fe_2O_3 NPs partially alleviated intestinal shortening in UC mice, whereas APTS-Fe_2O_3 NPs did not lead to significant improvement (Fig. 2E). However, no significant reduction in intestinal mass was observed across all groups (Fig. 2F). Furthermore, the colonic mucosal damage index (CMDI) results indicated that all four types of modified Fe_2O_3 NPs significantly ameliorated colonic mucosal injury in UC mice (Fig. 2G).

Histopathological analysis demonstrated that mice treated with γ-Fe_2O_3, PLL-Fe_2O_3, or DMSA-Fe_2O_3 NPs maintained intact intestinal mucosa architecture, devoid of bleeding, erosion, or ulceration. The underlying submucosa, muscularis, and serosa remained unaffected, with only mild inflammatory cell infiltration. Crypt architecture and goblet cell density were also similar to those in healthy controls. In contrast, mice treated with APTS-Fe_2O_3 NPs displayed significant mucosal erosion, edema, and dense inflammatory infiltration in both the lamina propria and submucosa (Fig. S3A in Supporting information), indicating a comparatively weaker anti-inflammatory effect.

Mast cells (MCs), which constitute approximately 15% of mononuclear cells in the lamina propria and submucosa of the gastrointestinal mucosa, are also present in the epithelium, muscularis, and serosa [29–32]. Accumulating evidence indicates that MCs participate in a variety of gastrointestinal physiological and pathological processes, including epithelial barrier function, mucosal immunity, host defense against bacterial, intestinal motility, and visceral sensitivity regulation [33–35]. Toluidine blue staining was employed to evaluate MC distribution in the intestinal mucosa. Mice treated with γ-Fe_2O_3, PLL-Fe_2O_3, or DMSA-Fe_2O_3 NPs showed few MCs in the cecum, colon, and rectum, comparable to normal controls. In contrast, APTS-Fe_2O_3 NP-treated mice exhibited substantial MC accumulation in these intestinal regions (Fig. S3B in Supporting information). Given that MCs promote intestinal inflammation through the release of mediators such as cytokines, amines, and proteases (including key proteases tryptase and chymase in acute UC) [36–38], we therefore employed immunohistochemistry (IHC) to qualitatively evaluate the expression of tryptase and chymase in the cecum, colon, and rectum. The results revealed only minimal levels of MC-derived tryptase and chymase in the submucosa and lamina propria of mice treated with γ-Fe_2O_3, PLL-Fe_2O_3, or DMSA-Fe_2O_3 NPs, similar to the normal group. Conversely, abundant tryptase and chymase were detected in the corresponding intestinal layers of APTS-Fe_2O_3 NP-treated mice (Figs. S3C and D in Supporting information). Consistent with these findings, Western blot (WB) analysis further confirmed that γ-Fe_2O_3, PLL-Fe_2O_3, and DMSA-Fe_2O_3 NPs significantly downregulated MC-associated inflammatory proteins, while APTS-Fe_2O_3 NPs showed only a marginal effect (Fig. S2B in Supporting information). Serum inflammatory cytokines are recognized as indirect biomarkers for assessing intestinal inflammation and evaluating therapeutic outcomes in UC models [39]. We quantified the serum levels of TNF-α, IL-1β, IL-6, and IL-10, associated with the severity of acute UC. The results demonstrated that the expression levels of all inflammatory cytokines were significantly reduced in mice treated with γ-Fe_2O_3 NPs, APTS-Fe_2O_3 NPs, PLL-Fe_2O_3 NPs, and DMSA-Fe_2O_3 NPs compared to control group (Fig. 2H), indicating a systemic alleviation of inflammation. Notably, mice administered with APTS-Fe_2O_3 NPs exhibited slightly higher cytokine levels than those treated with the other three types of Fe_2O_3 NPs. Furthermore, Prussian blue staining and histopathological analysis revealed no evident iron accumulation or notable pathological alterations in major organs across all treatment groups, confirming the favorable biosafety profile of the synthesized Fe_2O_3 NPs (Fig. S4 in Supporting information).

To further explore the mechanism behind the therapeutic effects of Fe_2O_3 NPs, we simulated the gastrointestinal digestion process *in vitro* (Fig. 3A). Tracking the digestion of Fe_2O_3 NPs in mice revealed that all formulations largely retained their spherical morphology. However, after 4 h of digestion, the particle size increased approximately threefold compared to the initial size (Fig. S5A in Supporting information). TEM images showed varying degrees of nanoparticle aggregation and adsorption of gastrointestinal proteins and organic components, resulting in the formation of a visible protein corona on the nanoparticle surfaces (Fig. S5B in Supporting information). We further analyzed the adsorption kinetics of GI proteins throughout the simulated oral-gastric-intestinal digestion. During the gastric phase, protein adsorption gradually increased with digestion time, with γ-Fe_2O_3 and APTS-Fe_2O_3 NPs exhibiting notably higher adsorption capacities than PLL-Fe_2O_3 and DMSA-Fe_2O_3 NPs. Intestinal digestion triggered a dip-rise-plateau profile in protein adsorption dynamics. The initial decline correlates strongly with pH changes along the digestive tract. By the end of the process, no statistically significant differences in protein adsorption were observed among the surface-modified Fe_2O_3 NPs, suggesting saturation-limited adsorption behavior (Fig. S6A in Supporting information).

The differences in gastrointestinal protein adsorption among surface-modified Fe_2O_3 NPs were analyzed by liquid chromatography-tandem mass spectrometry (LC-MS/MS). To ensure data reliability, successful extraction of the protein corona was confirmed by inductively coupled plasma optical emission spectrometry (ICP-OES). Results showed significantly higher iron

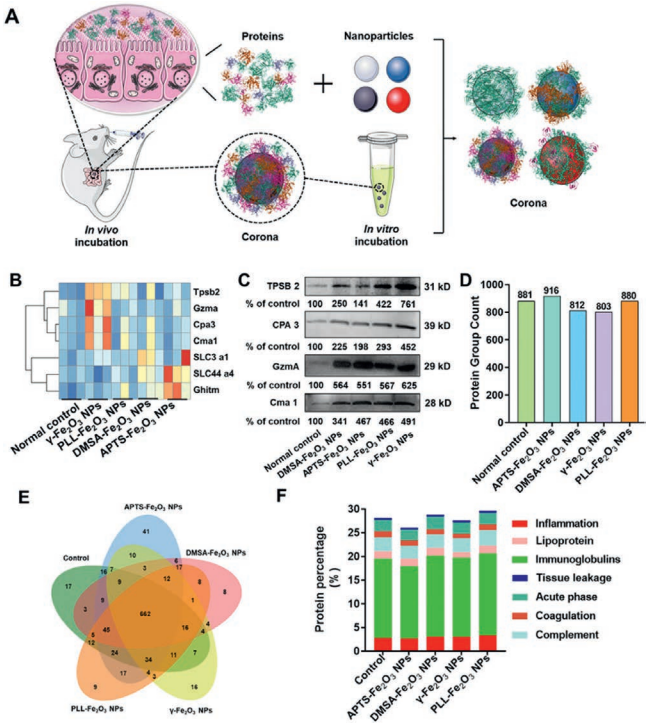


Fig. 3. The protein coronas analysis on the surface of Fe_2O_3 NPs. (A) The schematic figure of the gastrointestinal digestion process of Fe_2O_3 NPs in mice. (B) The LC-MS/MS results of protein in protein coronas. (C) Protein expression levels detected using WB. (D) Protein group counts. (E) Venn diagram of common and "exclusive" proteins identified from control, APTS-Fe_2O_3 NPs, DMSA-Fe_2O_3 NPs, γ-Fe_2O_3 NPs, and PLL-Fe_2O_3 NPs. (F) Classification of corona proteins based on physiological functions.

content in all treatment groups compared with the control, with each sample containing approximately 20 μg of iron (Fig. S6B in Supporting information). Given the close association between inflammatory proteins and the progression of UC, we focused on inflammation-related proteins. γ-Fe_2O_3 NPs exhibited the highest enrichment of inflammation-related proteins, including granzyme A (GzmA), tryptase beta 2 (TPSB2), carboxypeptidase A3 (CPA3), and chymase 1 (Cma1), whereas transport-related proteins were predominantly adsorbed by APTS-Fe_2O_3 NPs (Fig. 3B and Fig. S6C in Supporting information). WB validation further confirmed that all four types of Fe_2O_3 NPs adsorbed inflammation-related proteins to varying degrees, with APTS-Fe_2O_3 NPs showing notably higher adsorption of GzmA (Fig. 3C). Previous studies have reported that GzmA plays a protective role in IBD by inhibiting ferroptosis and enhancing intestinal epithelial barrier integrity [40].

Next, we evaluated the therapeutic efficacy of differently modified Fe_2O_3 NPs on IBD mice. First, we characterized the composition of corona proteins adsorbed onto the Fe_2O_3 NPs. As shown in Fig. 3D, we identified 881, 916, 812, 803, and 880 proteins in control, APTS-Fe_2O_3 NPs, DMSA-Fe_2O_3 NPs, γ-Fe_2O_3 NPs, and PLL-Fe_2O_3 NPs, respectively. Among them, the APTS-Fe_2O_3 NPs group exhibited the highest number of identified proteins. Correspondingly, Venn diagram analysis revealed that APTS-Fe_2O_3 NPs had more unique proteins, with 662 proteins common to all groups (Fig. 3E). Moreover, we observed a predominant adsorption of low molecular weight proteins (0–60 kDa) across all NP types (Fig. S6D in Supporting information). In addition, functional classification analysis of the proteins identified in each group demonstrated that the APTS-Fe_2O_3 NPs exhibited the lowest abundance of inflammation- and immune-related proteins (Fig. 3F). This finding offers a plausible explanation for the relatively poor therapeutic performance of APTS-Fe_2O_3 NPs in treating IBD.

To corroborate the *in vivo* findings, we simulated the oral-gastric-intestinal digestion of Fe_2O_3 NPs *in vitro* using artificial digestive fluids. The results demonstrated comparable morphological stability and time-dependent particle growth across all surface-modified Fe_2O_3 NPs, with no notable degradation observed (Figs. S7A and B in Supporting information). Zeta potential analysis uncovered distinct patterns of charge variation during the digestive process. Specifically, γ-Fe_2O_3, PLL-Fe_2O_3, and DMSA-Fe_2O_3 NPs exhibited a "decrease-increase-decrease" trend from the oral to gastric to intestinal phases. In contrast, APTS-Fe_2O_3 NPs displayed a consistently declining trend ("decrease-decrease-decrease", Fig. S7C in Supporting information). These differential behaviors reflect the distinct surface chemistries of the NPs and their dynamic interactions with the changing digestive microenvironment [41,42]. The initial decrease in zeta potential is likely attributable to the adsorption of negatively charged salivary proteins. The subsequent increase during the gastric phase may be explained by protonation under acidic conditions [43,44]. The final decrease in the intestinal phase corresponded to deprotonation and adsorption of negatively charged bile salts and enzymes, promoting protein corona formation that may enhance immune evasion and retention at inflamed sites [45–48].

For APTS-Fe_2O_3 NPs, the continuous decline in zeta potential across the digestive phases can be attributed to the protonation behavior of surface amino groups under varying pH conditions. During the gastric phase, limited protonation due to the high pK_a of amines resulted in only a minor increase in positive charge, while sustained adsorption of negatively charged proteins and enzymes led to a steady potential decrease. In the subsequent intestinal phase, the alkaline environment further deprotonated the amino groups, promoting increased adsorption of negatively charged molecules and thus continuing the declining trend [48,49]. These distinctive interfacial interactions likely reduced electrostatic attraction between APTS-Fe_2O_3 NPs and the intestinal mucosa, impairing adhesion and retention capabilities [50,51]. This zeta potential profile may also account for the preferential enrichment of inflammation-associated proteins on γ-Fe_2O_3 NPs and transport-related proteins on APTS-Fe_2O_3 NPs. Consequently, APTS-Fe_2O_3 NPs may exhibit less efficient targeting and adsorb fewer inflammatory proteins, instead undergoing greater transport and systemic absorption. This provides a plausible explanation for the inferior amelioration of UC symptoms by APTS-Fe_2O_3 NPs compared to other formulations. Furthermore, no significant changes in the Fe 2p binding energy following gastrointestinal digestion, confirming the chemical stability of the Fe_2O_3 NPs without degradation (Fig. S7D in Supporting information).

Since orally administered NPs must across the intestinal barrier to be absorbed, we established a co-culture intestinal model incorporating Caco-2, HT29, and Raji B cells to better mimic the physiological complexity of the small intestine (Fig. 4A). Immunofluorescence imaging confirmed the presence of mucin (Muc-2) and M cells (Figs. 4B and C). TEM further revealed a cellular monolayer recapitulating key features of the small intestinal epithelium: Intestinal epithelial cells with distinct microvilli, goblet cells containing mucus vacuoles, and M cells exhibiting blunted and fused microvilli (Fig. 4D). The continuity and integrity of the Transwell culture were verified by transepithelial electrical resistance (TEER) measurements (Fig. S8A in Supporting information). Permeability assays demonstrated that the APTS-Fe_2O_3 NPs group led to significantly higher fluorescence intensity of Lucifer yellow in the lower chamber compared to other groups, suggesting enhanced disruption of tight junctions and increased epithelial permeability (Fig. S8B in Supporting information).

To elucidate the molecular mechanism of APTS-Fe_2O_3 NPs-induced permeability enhancement, we investigated the role of integrin-mediated signaling. Upon binding to integrin receptors,

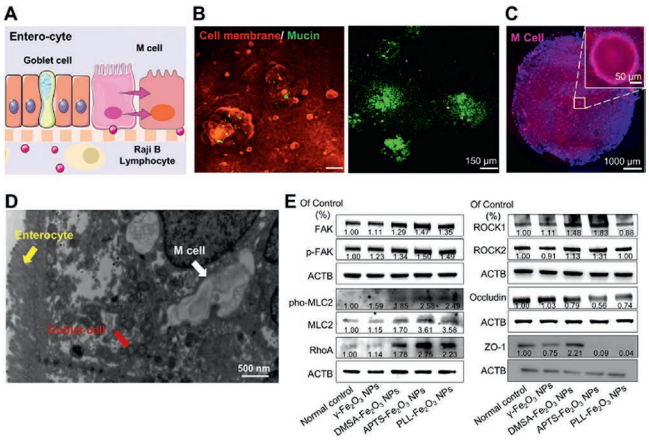


Fig. 4. Establishment of a multicellular model to elucidate the molecular mechanism of Fe_2O_3-induced permeability changes. (A) Triculture model schematic. (B, C) Mucin (green) and M cell (purple) were identified by immunofluorescence. (D) TEM of enterocyte, M cell, and goblet cell. Scale bar: 1 μm. (E) Protein expression levels detected using WB.

Fe_2O_3 NPs can trigger multiple signaling cascades that converge to activate myosin light-chain kinase (MLCK). The activated MLCK phosphorylates the myosin regulatory light chain, leading to cytoskeletal contraction and increased tension on tight junctions, thereby promoting their opening [52]. Specifically, APTS-Fe_2O_3 NPs induce the activation of FAK, a central kinase in integrin signaling that subsequently enhances the activity of both Rho associated coiled-coil containing protein kinase (ROCK) and MLCK. This signaling cascade facilitates actin cytoskeletal reorganization and disrupts the stability of tight junction proteins, including occludin and tight junction protein 1 (ZO-1), ultimately resulting in increased epithelial permeability (Fig. 4E and Fig. S8C in Supporting information).

In this study, we systematically evaluated how surface modifications of Fe_2O_3 NPs influence their therapeutic efficacy against IBD. Our results indicate that surface chemistry modification critically governs both the adsorption of gastrointestinal proteins and the cellular permeability of Fe_2O_3 NPs (Fig. S8D in Supporting information). Specifically, the protein corona that forms on nanoparticle surfaces from adsorbed biomolecules significantly influences their behavior within biological systems [53–55]. Each functionalization strategy confers distinct biological properties, shaping how the NPs interact with cells and tissues, cross epithelial barriers, and ultimately perform therapeutically [42,56,57]. Unlike conventional nanoparticle-based strategies for IBD treatment, which typically emphasize either iron supplementation or anti-inflammatory effects in isolation [58,59], our study introduces a novel dual-mechanism approach. The surface-modified Fe_2O_3 NPs offer both iron supplementation and inflammation modulation through selective adsorption of inflammatory proteins. Among the evaluated modifications, APTS-Fe_2O_3 NPs displayed distinct zeta potential transitions during gastrointestinal digestion and enhanced permeability across intestinal epithelial layers. These properties likely reduced their capacity to adsorb inflammatory proteins, ultimately leading to increased MC infiltration and elevated levels of inflammatory mediators in the intestinal tissue. This mechanism may explain the comparatively lower therapeutic efficacy of APTS-Fe_2O_3 NPs in IBD treatment relative to other surface-modified variants, underscoring the critical importance of tailoring nanoparticle surface characteristics to maximize therapeutic benefit. Overall, our study underscores the essential role of nanoparticle-protein interactions in guiding the rational design of nanomaterials for biomedical applications. By integrating both iron supplementation and inflammation modulation, our findings provide a comprehensive strategy for IBD therapy that extends beyond existing nanoparticle systems, opening new pathways toward more effective treatment options.

CRediT authorship contribution statement

Mengjie Wang: Writing – original draft, Methodology, Data curation. **Shilin Li:** Writing – original draft, Visualization, Methodology, Data curation. **Manman Ning:** Methodology, Data curation. **Yueguang Xue:** Visualization, Methodology, Data curation. **Ke Xu:** Visualization, Methodology. **Xinran Wang:** Visualization. **Shasha Jiang:** Writing – original draft, Visualization. **Yongfu Ma:** Writing – review & editing, Visualization. **Ying Liu:** Writing – review & editing, Project administration, Funding acquisition, Conceptualization.

Declaration of competing interest

The authors declare that they have no known competing financial interests or personal relationships that could have appeared to influence the work reported in this paper.

Acknowledgment

This work was supported by the National Natural Science Foundation of China (Nos. 22476031, 22027810).

Supplementary materials

Supplementary material associated with this article can be found, in the online version, at doi:10.1016/j.cclet.2025.112139.

References

[1] A.N. Ananthakrishnan, Nat. Rev. Gastroenterol. Hepatol. 12 (2015) 205–217.
[2] Y.Z. Zhang, Y.Y. Li, World J. Gastroenterol. 20 (2014) 91–99.
[3] S.C. Ng, H.Y. Shi, N. Hamidi, et al., Lancet 390 (2017) 2769–2778.
[4] C.N. Bernstein, F. Shanahan, Gut 57 (2008) 1185–1191.
[5] N.A. Molodecky, G.G. Kaplan, Gastroenterol. Hepatol. 6 (2010) 339–346.
[6] K.R. Nielsen, S.N. Lophaven, J. Midjord, et al., Inflamm. Bowel Dis. 31 (2025) 952–962.
[7] S. Danese, C. Fiocchi, N. Engl. J. Med. 365 (2011) 1713–1725.
[8] P. Rutgeerts, W.J. Sandborn, B.G. Feagan, et al., N. Engl. J. Med. 353 (2005) 2462–2476.
[9] W.J. Sandborn, B.G. Feagan, P. Rutgeerts, et al., N. Engl. J. Med. 369 (2013) 711–721.
[10] D.C. Baumgart, W.J. Sandborn, Lancet 380 (2012) 1590–1605.
[11] B. Huang, T. Yin, S. Fu, et al., Proc. Natl. Acad. Sci. U. S. A. 121 (2024) e2320482121.
[12] C. Yang, K. Sharma, R.J. Mow, et al., Cell. Mol. Gastroenterol. Hepatol. 18 (2024) 101333.
[13] W. Fu, L. Xu, Z. Chen, et al., J. Control. Release 363 (2023) 149–179.
[14] L. Wang, M. Yu, H. Yang, J. Inflamm. Res. 14 (2021) 1701–1716.
[15] P.G. Balaji, L.S. Bhimrao, A.K. Yadav, Mol. Neurobiol. 62 (2024) 184–220.
[16] A.N. Vaneev, O.A. Kost, N.L. Eremeev, et al., Biomedicines 9 (2021) 396.
[17] E. Tüzün, Chapter 15-nanotechnology-based management of neurological autoimmune diseases, in: Y. Gürsoy-Özdemir, S. Bozdağ-Pehlivan, E. Sekerdag (Eds.), Nanotechnology Methods for Neurological Diseases and Brain Tumors, Academic Press, 2017, pp. 279–290.
[18] M. Liu, Y. Wang, Y. Li, et al., MedComm Biomater. Appl. 4 (2025) e70012.
[19] T. Pan, D. Zhang, G. You, et al., Chin. Chem. Lett. 36 (2025) 109857.
[20] H. Hu, L. Yu, Z. Ding, et al., Chin. Chem. Lett. 34 (2023) 108592.
[21] T. Chen, W. Meng, Y. Li, et al., Nano Lett. 24 (2024) 7321–7331.
[22] Y. Dai, Y. Guo, W. Tang, et al., J. Nanobiotechnology 22 (2024) 252.
[23] E. Alphandéry, Drug Discov. Today 25 (2020) 141–149.
[24] Y. Ma, H. Wu, M. Jia, et al., J. Nanopart. Res. 26 (2024) 250.
[25] R. Wei, Y. Xu, M. Xue, J. Mater. Chem. B 9 (2021) 1965–1979.
[26] K. Xu, Y. Cui, B. Guan, et al., Nanoscale 16 (2024) 7786–7824.
[27] A. Abdelkawi, A. Slim, Z. Zinoune, Y. Pathak, Coatings 13 (2023) 1660.
[28] S.Z. Alshawwa, A.A. Kassem, R.M. Farid, et al., Pharmaceutics 14 (2022) 883.
[29] X.Y. You, H.Y. Zhang, X. Han, et al., Front. Pharmacol. 12 (2021) 659716.
[30] K.N. Dileepan, V.V. Raveendran, R. Sharma, et al., Front. Med. 10 (2023) 1213320.
[31] T. Leech, M. Peiris, J. Gastroenterol. 59 (2024) 165–178.
[32] D. Yazici, I. Ogulur, Y. Pat, et al., Semin. Immunol. 70 (2023) 101846.
[33] T.A. Suárez Vázquez, N. López López, M.C. Salinas Carmona, Front. Immunol. 15 (2024) 1360296.

[34] D.Elieh Ali Komi, K. Grauwet, Clin. Rev. Allergy Immunol. 54 (2018) 432–445.
[35] R. Berni Canani, M. Caminati, L. Carucci, I. Eguiluz-Gracia, Allergy 79 (2024) 1485–1500.
[36] B.Y. De Winter, R.M. van den Wijngaard, W.J. de Jonge, Biochim. Biophys. Acta 1822 (2012) 66–73.
[37] Ł. Gutowski, S. Kanikowski, D. Formanowicz, Life 13 (2023) 1690.
[38] V. Mariaule, A. Kriaa, S. Soussou, et al., Int. J. Mol. Sci. 22 (2021) 2817.
[39] M. Prakash, M.N. Chandraprabha, R. Hari Krishna, et al., Appl. Surf. Sci. Adv. 19 (2024) 100540.
[40] R. Niu, J. Lan, D. Liang, et al., Cell Commun. Signal. 22 (2024) 474.
[41] Y. Portilla, V. Mulens-Arias, N. Daviu, et al., ACS Appl. Mater. Interfaces 15 (2023) 35906–35926.
[42] J. Nowak-Jary, B. Machnicka, Int. J. Nanomedicine 18 (2023) 4067–4100.
[43] H.S. Ouandaogo, S. Diallo, E. Odari, J. Kinyu, PLoS One 19 (2024) e0295463.
[44] H. Pang, Y. Wu, Y. Chen, et al., Drug Deliv. Transl. Res. 14 (2024) 2345–2355.
[45] Y. Wang, L. Chen, Y. Wang, et al., J. Nanobiotechnology 21 (2023) 408.
[46] M. Chehelgerdi, M. Chehelgerdi, O.Q.B. Allela, et al., Mol. Cancer 22 (2023) 169.
[47] R. Liam-Or, F.N. Faruqu, A. Walters, et al., Nat. Nanotechnol. 19 (2024) 846–855.
[48] F. Veider, E. Sanchez Armengol, A. Bernkop-Schnürch, Small 20 (2024) e2304713.
[49] Z. Li, Y. Zhu, J.B. Matson, ACS Appl. Bio Mater. 5 (2022) 4635–4651.
[50] H.L. Huang, C.H. Lai, W.H. Tsai, et al., Life Sci. 337 (2024) 122379.
[51] C. Hu, G. He, Y. Yang, et al., Adv. Sci. 11 (2024) e2306070.
[52] T. Stalder, T. Zaiter, W. El-Basset, et al., Toxicology 481 (2022) 153353.
[53] C. Gunawan, M. Lim, C.P. Marquis, R. Amal, J. Mater. Chem. B 2 (2014) 2060–2083.
[54] C. Marques, G. Borchard, O. Jordan, Int. J. Pharm. 654 (2024) 123987.
[55] C. Pavón, E.M. Benetti, F. Lorandi, Langmuir 40 (2024) 11843–11857.
[56] M. Salehipour, S. Rezaei, J. Mosafer, et al., J. Nanopart. Res. 23 (2021) 48.
[57] G.M. Manoj, M. Shalini, K. Thenmozhi, et al., Appl. Surf. Sci. Adv. 21 (2024) 100608.
[58] A.X.X. Tan, B.Y.C. Ong, T. Dinesh, D.K. Srinivasan, Int. J. Mol. Sci. 26 (2025) 6465.
[59] S. Kaitha, M. Bashir, T. Ali, World J. Gastrointest. Pathophysiol. 6 (2015) 62–72.